EUROPEAN JOURNAL OF PURE AND APPLIED MATHEMATICS
2025, Vol. 18, Issue 4, Article Number 6642
ISSN 1307-5543 – ejpam.com
Published by New York Business Global

Simulating Arterial Blood Flow Using Finite Volume Conservation Element and Solution Element Scheme

Saqib Zia[1,*], Aqsa Qandeel[1], Asad Rehman[2], Sidrah Ahmed[3], Munshoor Ahmed[1], Wei Sin Koh[4]

[1] *Department of Mathematics, COMSATS University Islamabad, Park Road Chak Shehzad, Islamabad, Pakistan*
[2] *Department of Information Technology, Pothohar Campus Gujar Khan, University of the Punjab, Pakistan*
[3] *Department of Mathematics, Basic Sciences and Humanities, Sukkur IBA University, Sukkur, Pakistan*
[4] *INTI International University, Persiaran Perdana BBN Putra Nilai, 71800 Nilai, Negeri Sembilan, Malaysia*

Abstract. This article investigates the numerical approximation of blood flow in arteries with spatially varying stiffness and resting cross-sectional areas. The underlying model is formulated to preserve steady-state solutions by accurately balancing non-zero fluxes with corresponding source terms. The study focuses on addressing the numerical challenges posed by the model's complexity. To overcome these difficulties, a Conservation Element and Solution Element (CE/SE) scheme is employed, ensuring the preservation of the steady-state condition associated with zero discharge. The proposed scheme effectively minimizes numerical oscillations and dissipation, delivering improved accuracy and robustness compared to conventional methods. Its performance is evaluated through several benchmark cases from the existing literature, with results compared against those obtained using the Central Scheme.

2020 Mathematics Subject Classifications: 65N30, 74S05, 76M10

Key Words and Phrases: 1-D blood flow, CE/SE scheme, central scheme, KFVS scheme, non-conservative, hyperbolic systems, smart microgrids

1. Introduction

Simulation of blood flow has numerous applications in medical science, driven by the pulsatile nature of blood and the necessity to accurately capture wave propagation within

*Corresponding author.
DOI: https://doi.org/10.29020/nybg.ejpam.v18i4.6642

Email addresses: saqibzia81@hotmail.com (S. Zia), aqsaqandeel18@gmail.com (A. Qandeel), assad013@gmail.com (A. Rehman), dr.sidrah@iba-suk.edu.pk (S. Ahmed), manshoor@comsats.edu.pk (M. Ahmed), weisin.koh@newinti.edu.my (W. S. Koh)

arteries [1, 2]. The study of one-dimensional blood flow equations dates back to 1775, when Leonhard Euler first formulated them (as cited in [1]), highlighting the inherent challenges in their solution; see, for example, [2]. Since then, pulsatile wave flow has been extensively examined in seminal works, notably those of Pedley [3] and Lighthill [4]. Recent studies have made substantial progress in solving the governing systems of equations for arterial blood flow [5–17]. While advances in three-dimensional fluid–structure interaction models have been remarkable [18, 19], one-dimensional modeling remains indispensable particularly for analyzing complex arterial networks and venous systems [6–8, 20–23].

The shallow water equations (SWE), first formulated by Adhémar Barré de Saint-Venant in 1871 [24], have been extensively studied and applied across a wide range of fields. They are commonly used to model phenomena such as river flows [25], lake dynamics, dam-break scenarios, and tsunami propagation [26–28]. Incorporating source terms into the Saint-Venant equations, however, introduces numerical challenges, particularly in preserving steady-state solutions. To address this, Bermúdez and Vázquez [29, 30] proposed modifications to the Roe solver aimed at maintaining steady states. LeVeque [31] and Jin [32] developed exact and approximate Riemann solvers specifically designed for non-homogeneous problems, while other researchers [33, 34] proposed approaches based on solving the Riemann problem associated with the SWE. More recently, Delestre, Li, and collaborators [35–37] have applied finite volume schemes to solve the SWE for the simulation of blood flow in arteries.

This study extends a CE/SE scheme [38] to address the SWE's in a blood flow model for arteries. Unlike conventional methods, this scheme is specifically designed to overcome key limitations of existing approaches [38–41]. Its distinguishing characteristics include (i) a coherent treatment of time and space, (ii) the integration of conservation elements (CEs) and solution elements (SEs), and (iii) the ability to capture shocks without relying on Riemann solvers. The CE/SE scheme has been successfully applied in various domains, including unsteady flow dynamics [38–40], aeroacoustics [42], diffusion processes [41], and more [43–47]. The performance of the CE/SE scheme is assessed by comparing its results with those derived from the staggered central scheme [48].

Notation

Symbol	Description
x	Spatial coordinate along the vessel
t	Time
$A_v(x,t)$	Cross-sectional area of the vessel
$A_0(x)$	Resting cross-sectional area of the vessel
$R_v(x,t)$	Vessel radius
R_v^0	Resting vessel radius
$Q_v(x,t)$	Discharge (volume flow rate)
$\bar{u}(x,t)$	Mean blood velocity across the section
$u(x,t,r)$	Longitudinal velocity at radial location r
ρ	Blood density
ν_b	Blood viscosity
$C_f = 8\pi\nu_b$	Friction coefficient
k	Arterial stiffness (elasticity parameter)
W	Conserved variable vector
$F(W)$	Flux vector
$\tau(W)$	Source term vector
$J(W)$	Jacobian matrix of flux
λ_1, λ_2	Eigenvalues (wave speeds $u \pm c$)
u	Average flow velocity (Q_v/A_v)
c	Wave propagation speed
Ω, V	Conservation/solution element regions
h_i, f_i	Auxiliary flux/state vectors in CE/SE scheme
$\Delta x, \Delta t$	Spatial and temporal step sizes
α	Limiter parameter in slope reconstruction
N	Number of computational grid cells
L	Length of the computational domain
ϵ	Perturbation amplitude for test problems
ΔR	Amplitude of radius variation (aneurysm cases)
Φ	Prescribed wave profile function
c_0	Characteristic wave speed
Q_{amp}	Amplitude of imposed discharge wave
ω	Angular frequency of periodic inflow
T_{pulse}	Period of pulse wave
k_r, k_j	Real and imaginary components of wave number

Table 1: List of symbols and notations used throughout the paper.

2. Mathematical Equations

The one-dimensional mathematical equations are derived from the Navier–Stokes (NS) equations by applying the long-wave approximation [49, 50]. In this formulation, transverse and longitudinal viscous effects are considered negligible. Incompressibility is ensured by assuming uniform pressure across each cross-section, while the flow variables vary only along the longitudinal coordinate (see Figure.1). The governing equations of the model are given by:

$$\begin{cases} \frac{\partial A_v}{\partial t} + \frac{\partial Q_v}{\partial x} = 0 \\ \frac{\partial Q_v}{\partial t} + \frac{\partial (\frac{{Q_v}^2}{A_v})}{\partial x} + \frac{A_v}{\rho}\frac{\partial p}{\partial x} = -C_f \frac{Q_v}{A_v}. \end{cases} \tag{1}$$

Here, $A_v(x,t) = \pi {R_v}^2$ depicts the cross-sectional area of the vessel, R_v represents vessel radius,, $Q_v(x,t) = A_v(x,t)\bar{u}(x,t)$ signifies the discharge, $\bar{u}(x,t)$, is the mean flow velocity, ρ signifies blood density and $C_f = 8\pi\nu_b$ where ν_b defined as viscosity.

$$\bar{u}(x,t) = \int_0^{R_v} \frac{2\pi u(t,x,r) r dr}{\pi {R_v}^2}$$

with $u(t,x,r)$ signifies the longitudinal velocity.

The 1D mathematical equations (1) can also be written as, By using the following relation,

$$\bar{u}(x,t) = \int_0^{R_v} \frac{2\pi u(t,x,r) r dr}{\pi {R_v}^2}$$

with $A_v = \pi {R_0}^2$, A_0 and k represent the resting cross-sectional area and arterial stiffness, respectively. The 1-D blood flow model (1) can be written in the following form,

$$\begin{cases} \frac{\partial A_v}{\partial t} + \frac{\partial Q_v}{\partial x} = 0 \\ \frac{\partial Q_v}{\partial t} + \frac{\partial (\frac{{Q_v}^2}{A_v} + \frac{k}{3\rho\sqrt{\pi}} {A_v}^{3/2})}{\partial x} = \frac{kA_v}{2\rho\sqrt{\pi}\sqrt{A_0}}\frac{\partial A_0}{\partial x} - C_f \frac{Q_v}{A_v}. \end{cases} \tag{2}$$

In compact form,

$$\partial_t W + \partial_t F = \tau \tag{3}$$

where W depicts conserved variable vectors, $F = F(W)$ is flux vector and $\tau = \tau(W)$

$$\mathbf{W} = \begin{pmatrix} A_v \\ Q_v \end{pmatrix}, \quad \mathbf{F}(\mathbf{W}) = \begin{pmatrix} Q_v \\ \frac{{Q_v}^2}{A_v} + \frac{k}{3\rho\sqrt{\pi}} {A_v}^{3/2} \end{pmatrix} \tag{4}$$

$$\tau(\mathbf{W}) = \begin{pmatrix} 0 \\ \frac{kA_v}{\rho\sqrt{\pi}}\partial_x\sqrt{A_0} - C_f\frac{Q_v}{A_v} \end{pmatrix}. \tag{5}$$

The system is hyperbolic for $Av > 0$. Therefore, we have

$$\frac{\partial F(W)}{\partial x} = \begin{pmatrix} 0 & 1 \\ \frac{k\sqrt{A_v}}{2\rho\sqrt{\pi}} - \frac{Q_v^2}{A_v^2} & \frac{2Q_v}{A_v} \end{pmatrix} \cdot \frac{\partial}{\partial x}\begin{pmatrix} A_v \\ Q_v \end{pmatrix} = J(W) \cdot \frac{\partial W}{\partial x}$$

The two eigenvalues of the Jacobian matrix $J(W)$ are real and distinct. $\lambda_1 = \dfrac{Q_v}{A_v} - \sqrt{\dfrac{kR_v}{2\rho}} = u - c$ and $\lambda_2 = \dfrac{Q_v}{A_v} + \sqrt{\dfrac{kR_v}{2\rho}} = u + c$.

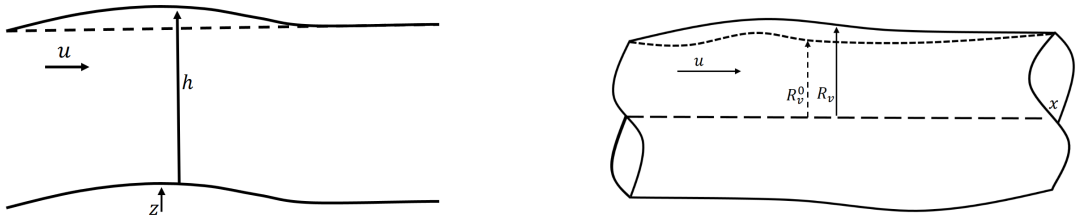

Figure 1: The left figure illustrates blood flow in which u, R_ν, and R_ν^0 represent the velocity, radius, and radius at rest of the flow, respectively. The right figure depicts the shallow flow in which u, h, and z represent the velocity, height, and bottom topography of the flow, respectively.

3. Derivation of the scheme

The CE/SE scheme serves as a powerful numerical tool for addressing various problems in continuum mechanics. Originally developed for the numerical computation of conservation laws governing fluid dynamics, this scheme stands out for its ability to minimize numerical dissipation and oscillations effectively. Here, 1-D CE/SE method [38] is derived for equations (1)–(5). Let $(x_0, x_1) = (t, x)$ be the coordinates in 2-D Cartesian space (E_2). The following form can be derived by applying the Gauss divergence theorem to Eq. (3).

$$\oint_{\Omega(\nu)} h_i \cdot \mathrm{d}S = \int_V \tau_i \, \mathrm{d}V \tag{6}$$

in which (a) $h_i \coloneqq (W_i, F_i)^T, \quad i = 1, 2$, i.e., for all $i = 1, 2$, W_i and F_i are the elements of h_i in the specified t and x directions, (b) $\mathrm{d}S \coloneqq \mathrm{d}\sigma \, n$, where $\mathrm{d}\sigma$ represents the area and n is the unit outward normal vector to the surface component on $\Omega(V)$. We divide the whole domain into a union of conservation elements (CE's) and solution elements (SE's). Equation (6) is applied over the space-time region CE, which accommodates discontinuities in the flow variables.

For each $j, k = 0, \pm\frac{1}{2}, \pm 1, \pm\frac{3}{2}, \ldots$, there exists an SE corresponding to each (j, k), as depicted in Fig. 1 (dashed curve). For any point $(x, t) \in \mathrm{SE}_j^k$, f_i, h_i, and W_i are estimated by f_i^*, h_i^*, and W_i^*, and these variables take the following form:

$$W_i^*(x,t)_j^n := (W_i)_j^k + (W_{it})_j^k \, (t - t^k) + (W_{ix})_j^k \, (x - x_j), \tag{7}$$

and

$$f_i^*(x,t)_j^n := (f_i)_j^k + (f_{it})_j^k \, (t - t^k) + (f_{ix})_j^k \, (x - x_j), \tag{8}$$

Moreover,

$$\tau_i^*(x,t)_j^n := \tau\big(W_i^*, W_{ix}^*\big). \tag{9}$$

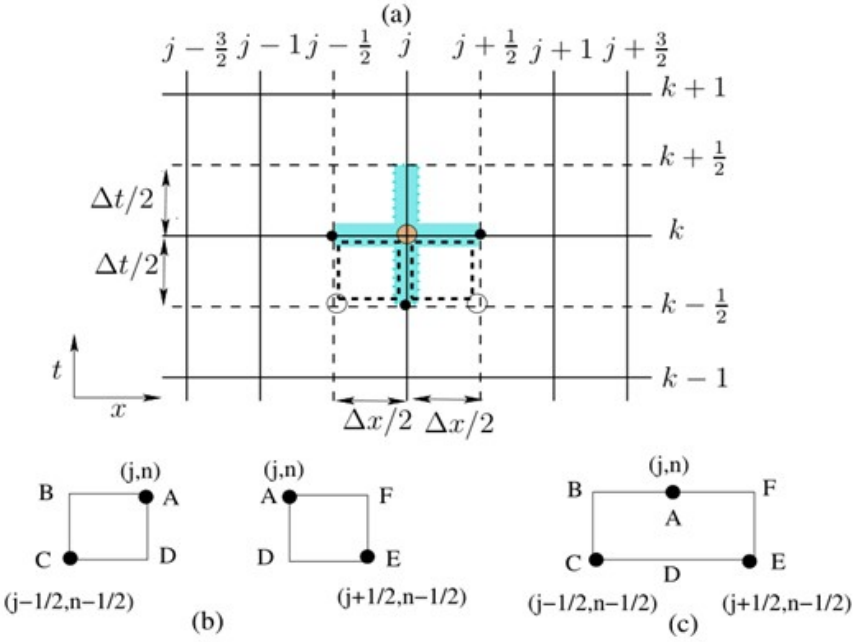

Figure 2: Staggered space-time grid

Using the chain rule, we acquire

$$(f_{ix})_j^k = \sum_{n=1}^{4} (f_{i,n})_j^k \ (W_{nx})_j^k, \tag{10}$$

$$(f_{it})_j^k = \sum_{n=1}^{4} (f_{i,n})_j^k \ (W_{nt})_j^k, \tag{11}$$

where

$$f_{i,n} := \frac{\partial f^i}{\partial W_n}, \quad i,n = 1,2. \tag{12}$$

Note that $(W_i)_j^k$, $(W_{ix})_j^k$, and $(W_{it})_j^k$ are constants in $\mathrm{SE}(j,k)$. The numerical equivalents of these values are W_i, $\frac{\partial W_i}{\partial x}$, and $\frac{\partial W_i}{\partial t}$ at (x_j, t^k). Since $h_i \triangleq (W_i, f_i)$, we define

$$h_{i\,j}^{*k} := \left(W_{i\,j}^{*k}, f_{i\,j}^{*k}\right)^T. \tag{13}$$

Moreover, for any $(x,t) \in \mathrm{SE}_j^k$, W_i^*, f_i^*, and τ_i^* satisfy Eq. (3) under the assumption of smoothness:

$$\frac{\partial W_i^*(x,t)}{\partial t} + \frac{\partial f_i^*(x,t)}{\partial x} = \tau_i^*(x,t). \tag{14}$$

Using Eqs. (7) and (8), Eq. (14) becomes

$$(W_{it})_j^k = -(f_{ix})_j^k + \tau_i\big((W_i)_j^k, (W_{ix})_j^k\big). \tag{15}$$

We notice that $(f_i)_j^k$ depends on $(W_i)_j^k$, $(f_{ix})_j^k$ depends on $(W_i)_j^k$ and $(W_{ix})_j^k$, $(f_{it})_j^k$ depends on $(W_i)_j^k$ and $(W_{it})_j^k$, and Q_i depends on $(W_i)_j^k$ and $(W_{ix})_j^k$. See [46] for details. Here, fluxes are computed by the AUSMV method [51].

Using Eqs. (7)–(9) and (13), we get

$$\begin{aligned}(W_i)_j^k &= (W_i)_{j\pm\frac{1}{2}}^{k-\frac{1}{2}} \mp \frac{\Delta x}{4}\left[(W_{ix})_{j\pm\frac{1}{2}}^{k-\frac{1}{2}} + (W_{ix})_j^k\right] \\ &\quad \mp \frac{\Delta t}{\Delta x}\left[(f_i)_{j\pm\frac{1}{2}}^{k-\frac{1}{2}} - (f_i)_j^k\right] \\ &\quad \mp \frac{\Delta t^2}{4\,\Delta x}\left[(f_{it})_{j\pm\frac{1}{2}}^{k-\frac{1}{2}} + (f_{it})_j^k\right] \pm \left[(Q_l)_{j\pm\frac{1}{2}}^{k-\frac{1}{2}} - (Q_l)_j^k\right].\end{aligned} \tag{16}$$

The summation gives

$$(W_i)_j^k = \frac{1}{2}\Big[(W_i)_{j-\frac{1}{2}}^{k-\frac{1}{2}} + (W_i)_{j+\frac{1}{2}}^{k-\frac{1}{2}} + (S_i)_{j-\frac{1}{2}}^{k-\frac{1}{2}} - (S_{il})_{j+\frac{1}{2}}^{k-\frac{1}{2}}\Big] + (Q_l)_{j+\frac{1}{2}}^{k-\frac{1}{2}} - (Q_l)_{j-\frac{1}{2}}^{k-\frac{1}{2}}, \tag{17}$$

where

$$(S_i)_{j\pm\frac{1}{2}}^{k-\frac{1}{2}} = \frac{\Delta x}{4}(W_{ix})_{j\pm\frac{1}{2}}^{k-\frac{1}{2}} + \frac{\Delta t}{\Delta x}(F_i)_{j\pm\frac{1}{2}}^{k-\frac{1}{2}} + \frac{\Delta t^2}{4\,\Delta x}(f_{it})_{j\pm\frac{1}{2}}^{k-\frac{1}{2}}. \tag{18}$$

The following slope limiter is used to overcome oscillations:

$$(W_{ix})_j^k = U_i\left((W_{ix_-})_j^k,\, (W_{ix_+})_j^k\,;\, \alpha\right), \quad i = 1, \ldots, 4, \tag{19}$$

where $\alpha \geq 0$ is a parameter, and

$$U_i = \frac{x_- \,|x_+|^\alpha + x_+ \,|x_-|^\alpha}{|x_+|^\alpha + |x_-|^\alpha}. \tag{20}$$

Furthermore,

$$\big(W_{ix_+}\big)_j^k = \frac{(W_i')_{j+\frac{1}{2}}^k - (W_i)_j^k}{\Delta x/2}, \tag{21}$$

$$\big(W_{ix_-}\big)_j^k = \frac{(W_i)_j^k - (W_i')_{j-\frac{1}{2}}^k}{\Delta x/2}, \tag{22}$$

with

$$\big(W_i'\big)_{j\pm\frac{1}{2}}^k = (W_i)_{j\pm\frac{1}{2}}^{k-\frac{1}{2}} + \frac{\Delta t}{2}\,(W_{it})_{j\pm\frac{1}{2}}^{k-\frac{1}{2}}, \quad i = 1, \ldots, 4. \tag{23}$$

Combining Eqs. (17) and (19) completes the derivation of the 1-D CE/SE scheme.

4. Numerical test problems

This section provides a variety of numerical test cases from literature.

Problem 1: The ideal tourniquet

This case study is also addressed in [37, 52]. A tourniquet is applied and then immediately removed. The following initial conditions at t=0 are considered,

$$A_v(x) = \begin{cases} \pi(R_v^L)^2 \text{ if } x \leq 0, \\ \\ \pi(R_v^R)^2 \text{ otherwise.} \end{cases} \qquad \text{and } Q_v = 0.$$

The computational domain $\left[-\frac{4}{100}, \frac{4}{100}\right]$ m is divided into 200 grid points. Furthermore, we take the following values of the parameters:

$$k = 1.0{\times}10^7\,\mathrm{kg\,m^{-2}\,s^{-2}}, \quad \rho = 1.060{\times}10^3\,\mathrm{kg\,m^{-3}}, \quad R_v^L = 5.0{\times}10^{-3}\,\mathrm{m}, \quad R_v^R = 4.0{\times}10^{-3}\,\mathrm{m}.$$

The results, shown in Figure 3, clearly indicate that the CE/SE scheme closely matches the reference solution. Furthermore, the L^1-errors for all schemes are listed in Table 1, demonstrating that the CE/SE scheme achieves lower errors than the other methods.

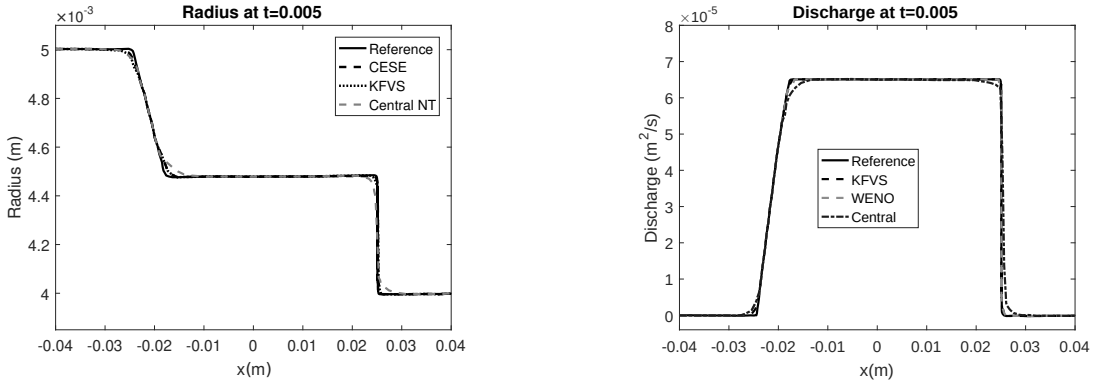

(a) Radius R_v (b) Discharge $Q_v(x)$

Figure 3: The numerical solutions of the ideal tourniquet problem on a mesh with 200 cells at $t = 0.005$ seconds. (a) Radius R_v, (b) Discharge $Q_v(x)$.

Problem 2: Wave Equation

The purpose of this test study is to check the numerical scheme's capability in simulating perturbed steady solutions. The initial conditions are as follows [36, 37]: The cross-sectional area is defined as

$$A_v(x) = \begin{cases} \pi(R_v^0)^2, & \text{if } x \in \left[0, \frac{4L}{10}\right] \cup \left[\frac{6L}{10}, L\right], \\ \\ \pi(R_v^0)^2 \left[1.0 + \frac{1}{200}\sin\left(\pi \frac{x - \frac{4L}{10}}{\frac{2L}{10}}\right)\right]^2, & \text{if } x \in \left[\frac{4L}{10}, \frac{6L}{10}\right], \end{cases}$$

Table 2: Problem 3: Comparison of L^1-errors in the schemes.

Radius			
N	CE/SE	KFVS	Central(NT)
50	0.0141	0.2011	0.4510
100	0.0043	0.0181	0.3110
200	0.0022	0.0054	0.3139
400	0.0012	0.0028	0.2035
800	6.7120×10^{-4}	0.0023	0.1540
1600	2.4123×10^{-4}	6.4235×10^{-4}	0.0139

where the domain $[0, 0.16]$ is divided into 200 points. Furthermore, we take:

$$Q(x) = 0\,\mathrm{m^3\,s^{-1}}, \quad k = 1.0{\times}10^8\,\mathrm{kg\,m^{-2}\,s^{-2}}, \quad \rho = 1.060{\times}10^3\,\mathrm{kg\,m^{-3}}, \quad R_v^0 = 4.0{\times}10^{-3}\,\mathrm{m}, \quad L = 1.6{\times}10^{-1}\,\mathrm{m}.$$

The exact solutions are given by [37]:

$$\begin{cases} R_v(x,t) = R_v^0 + \frac{1}{400}\left[\Phi(x - c_0 t) + \Phi(x + c_0 t)\right], \\ u(x,t) = -\frac{c_0}{400 R_v^0}\left[-\Phi(x - c_0 t) + \Phi(x + c_0 t)\right]. \end{cases}$$

The numerical results are generated using the CE/SE scheme and the staggered central scheme and are presented in Figure 4. Results computed on 200 cells are shown at $t = 0.002$, 0.004, and 0.006 s. The outcomes from the proposed scheme closely match the reference solution.

Problem 3: The man at eternal rest

Here, we examine a non-flow scenario involving a variation in radius $R_0(x)$, representing the condition of a deceased individual with an aneurysm. The initial data are:

$$R_v = R_v^0 = \begin{cases} \tilde{R}, & \text{if } x \in [0, x_1] \cup [x_4, L], \\ \tilde{R} + 0.5\,\Delta R\left[\sin\left(\frac{x - x_1}{x_2 - x_1}\pi - \frac{\pi}{2}\right) + 1\right], & \text{if } x_1 \le x \le x_2, \\ \tilde{R} + \Delta R, & \text{if } x_2 \le x \le x_3, \\ \tilde{R} + 0.5\,\Delta R\left[\cos\left(\frac{x - x_3}{x_4 - x_3}\pi\right) + 1\right], & \text{if } x_3 \le x \le x_4. \end{cases}$$

The domain $[0, L]$ m is divided into 200 points. At $t = 0$, $u = 0$, the values of other parameters are:

$$k = 1.0{\times}10^8\,\mathrm{kg\,m^{-2}\,s^{-2}}, \quad \tilde{R} = 4.0{\times}10^{-4}\,\mathrm{m}, \quad \rho = 1.060{\times}10^3\,\mathrm{kg\,m^{-3}}, \quad \Delta R = 1.0{\times}10^{-3}\,\mathrm{m},$$

$$L = 1.4{\times}10^{-1}\,\mathrm{m}, \quad x_1 = 1.0{\times}10^{-2}\,\mathrm{m}, \quad x_2 = 3.05{\times}10^{-2}\,\mathrm{m}, \quad x_3 = 4.95{\times}10^{-2}\,\mathrm{m}, \quad x_4 = 7.0{\times}10^{-3}\,\mathrm{m}.$$

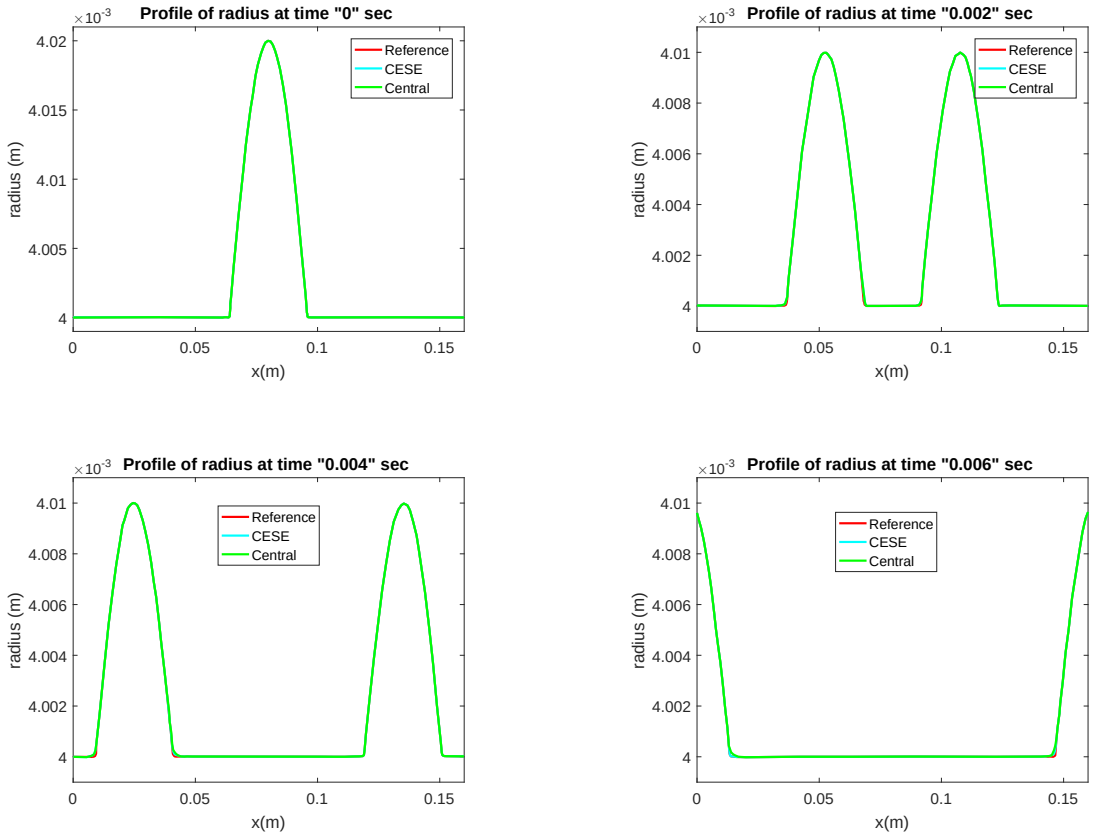

Figure 4: Results of problem 2. From top left to bottom right: (a) Initial radius (Top left) (b) Radius at $t = 0.002s$ (Top right) (c)Radius at $t = 0.004s$ (Bottom left) (d) Radius at $t = 0.006s$ (Bottom right)

It is evident from Figure. 5 that our suggested scheme maintains the well-balanced property.

Problem 4: Propagation of a pulse to an expansion

Initially, we start by analyzing the case of a pulse in a section R_v^R that is expanding: $A_v^L > A_v^R$. The other related parameters are:

$$\rho = 1060\text{kg m}^{-3}, \quad k = 1.0 \times 10^8 \text{ kg m}^{-2}\text{ s}^{-2}, \quad R_v^L = 5.0 \times 10^{-3} \text{ m},$$
$$R_v^R = 4.0 \times 10^{-3} \text{ m}, \quad L = 1.6 \times 10^{-1} \text{ m}, \quad \Delta R = 1.0 \times 10^{-3} \text{ m}.$$

On a small scale, we take the following decreasing shape:

$$R_v^0(x) = \begin{cases} R_v^R + \Delta R & \text{if } x \in [0,\ x_1], \\ R_v^R + \frac{\Delta R}{2}[1.0 + \cos\left(\frac{x - x_1}{x_2 - x_1}\pi\right)] & \text{if } x \in [x_1,\ x_2], \\ R_v^R & \text{else,} \end{cases}$$

with $\epsilon = 5.0 \times 10^{-3}$.

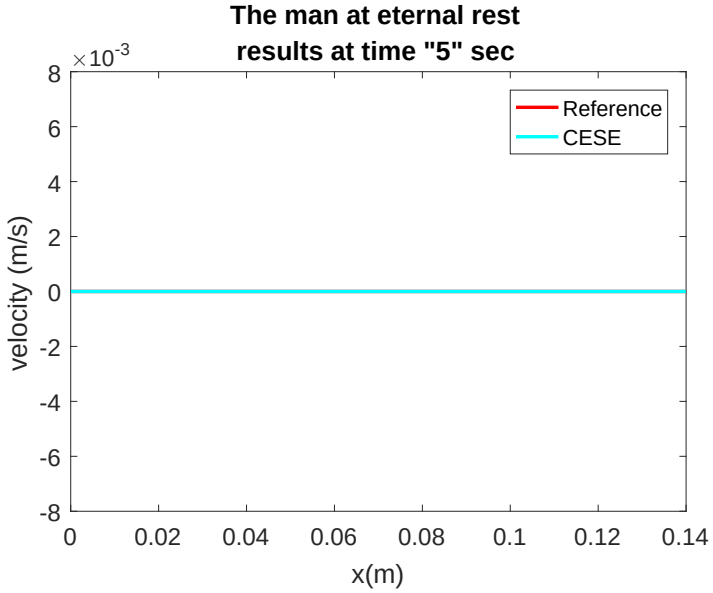

Figure 5: Representation of well-balanced CE/SE scheme.

In Figure. 6, we compare the numerical outcomes to the reference solutions at $t = 0.002$s and $t = 0.006$s. The numerical solutions greatly approximate the referenced ones and are equivalent to those in [36].

Problem 5: Propagation of a pulse from an expansion

In this case, all of parameters of problem 4 are considered except the initial radius, however, pulse propagation is considered from an expansion. Initially, the radius at $t = 0$ is given as,

$$R_v(x) = \begin{cases} R_v^0(x)[1.0 + \epsilon \sin\ \left(\frac{100}{20L}\pi(x - \frac{15L}{100})\right)] \text{ if } x \in\ [\frac{15L}{100},\ \frac{35L}{100}], \\ R_v^0(x) \text{ else.} \end{cases}$$

Here, $\epsilon = 5.0 \times 10^{-3}$. The numerical outcomes at $t = 0.002$s and $t = 0.006$s are depicted in Fig. 7. One observes that the numerical solutions closely predict the referenced ones and are analogous to those in [36].

Problem 6: Wave damping

This test problem is similar to the Womersley [53] problem. An investigation of viscous damping term in the linearized momentum equation is carried out in this problem. A periodic signal with a constant segment at rest is considered at the inflow. The model is given by [37],

$$\begin{cases} \partial_t A + \partial_x Q = 0, \\ \partial_t Q + \partial_x(\frac{Q^2}{A} + \frac{k}{3\rho\sqrt{\pi}}A^{\frac{3}{2}}) = \frac{kA}{\rho\sqrt{\pi}}\partial_x(\sqrt{A_0}) - C_f\frac{Q}{A}. \end{cases} \tag{24}$$

In the above model, $C_f = 8\pi v$, the viscosity of the blood is represented by v. The domain

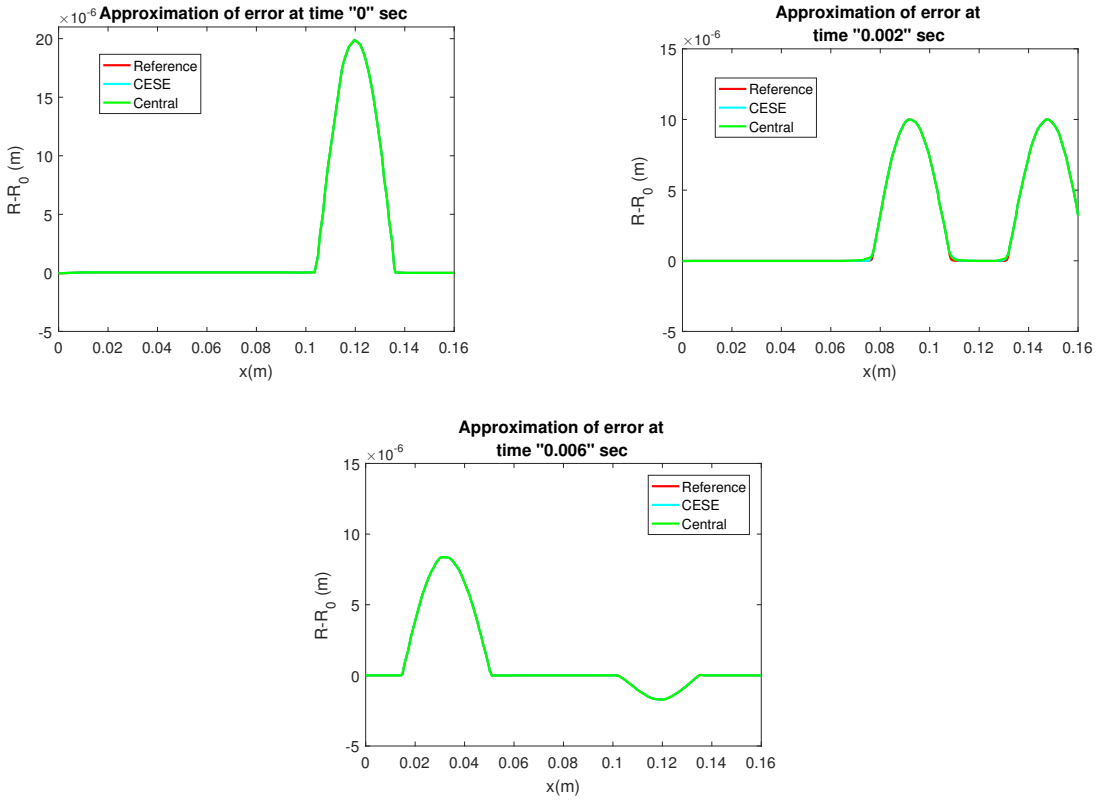

Figure 6: The numerical solutions of the propagation of a pulse to an expansion on a mesh with 100 cells: (a) Initial errors $R - R_0$ at $t = 0.0$s (Top left) (b) Errors $R - R_0$ at $t = 0.002$s (Top right) (c)Errors $R - R_0$ at $t = 0.004$s (Bottom)

$[0, 3]$ is divided into 200 grid points. The radius R_v and discharge Q_v at $t = 0$ are,

$$A_v(x) = \pi(R_v^0)^2, \qquad Q_v(x) = 0.$$

The values of other related parameters are: $\rho = 1060$ kg.m^{-3}, $k = 1 \times 10^8$ Pa.m^{-1}, $R_v^0 = 4 \times 10^{-3}$ m. For this example, the solution is obtained up to $t = 25$ s. A damping wave is obtained in the domain [36]

$$Q(t,\ x) = \begin{cases} 0 & \text{if } k_r x > \omega t, \\ Q_{\text{amp}} \sin(\omega t - k_r x) e^{k_i x} & \text{if } k_r x \leq \omega t, \end{cases} \tag{25}$$

with

$$k_r = [\frac{\omega^4}{c_0^4} + (\frac{\omega C_f}{\pi {R_v^0}^2 c_0^2})^2]^{\frac{1}{4}} \cos(\frac{1}{2}\arctan(-\frac{C_f}{\pi {R_v^0}^2 \omega})) \ ,$$

$$k_j = [\frac{\omega^4}{c_0^4} + (\frac{\omega C_f}{\pi {R_v^0}^2 c_0^2})^2]^{\frac{1}{4}} \sin(\frac{1}{2}\arctan(-\frac{C_f}{\pi {R_v^0}^2 \omega})) \ ,$$

$$\omega = 2\pi / T_{\text{pulse}} = 2\pi / 0.5s,$$

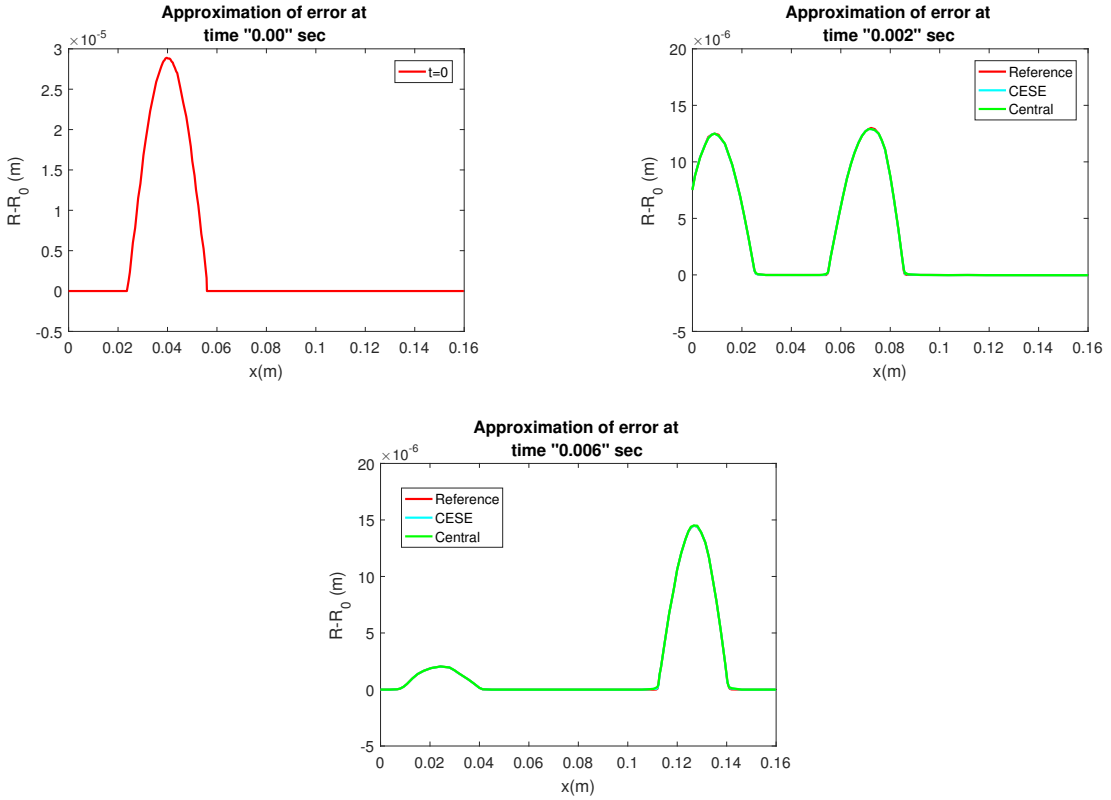

Figure 7: The numerical solutions of the propagation of a pulse from an expansion on a mesh with 100 cells (a) Initial errors $R - R_0$ at $t = 0.0$s (b) Errors $R - R_0$ at $t = 0.002$s (c) Errors $R - R_0$ at $t = 0.004$s.

$$c_0 = \sqrt{\frac{\sqrt{A_0}k}{2\sqrt{\pi}\rho}} = \sqrt{\frac{R_v^0 k}{2\rho}}.$$

At $x = 0$ the incoming discharge is,

$$Q_b(0,t) = Q_{\text{amp}} \sin(\omega t) m^3/s,$$

where, $Q_{\text{amp}} = 3.45 \times 10^{-7}\text{m}^3.\text{s}^{-3}$ being the amplitude of inflowing discharge.

The results are presented in Fig. 8. The CE/SE scheme agree well with the referenced solutions and those presented in [36].

5. Conclusions

In this study, a one-dimensional blood flow model for arterial circulation was numerically investigated using the conservation element and solution element(CE/SE) scheme. The inclusion of non-conservative terms in the governing equations complicates the balance between fluxes and source terms, introducing significant numerical challenges. The CE/SE scheme proved efficient in addressing these difficulties by accurately capturing sharp discontinuities while maintaining local and global conservation. This capability makes it

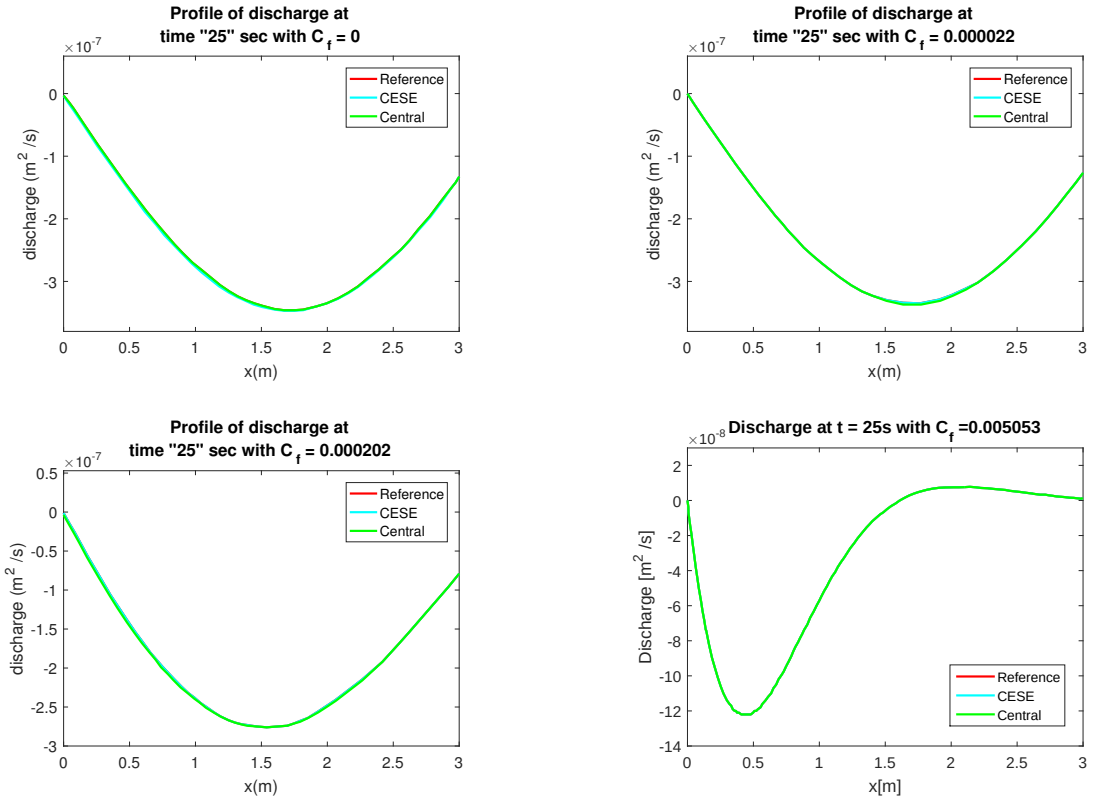

Figure 8: The numerical solutions of the wave damping on a mesh with 200 cells at t = 25 seconds. The damping of a discharge wave with $C_f = 0$ (upper left), $C_f = 0.000022$ (upper right), $C_f = 0.000202$ (lower left), and$C_f = 0.005053$ (lower right)

particularly suitable for wave phenomena in arterial systems that involve discontinuities or steep gradients, such as shock-like pulse waves and flow phase transitions. Numerical test cases demonstrated the robustness of the proposed approach under varying hemodynamic conditions, with the CE/SE scheme achieving superior accuracy and reduced oscillations compared to central and KFVS methods. Future work may extend this framework to more realistic physiological settings, including patient-specific arterial networks, viscoelastic wall models, and three-dimensional fluid–structure interactions. Such extensions will further enhance the applicability of the method in medical simulations and the study of cardiovascular pathologies.

References

[1] D. Xiu and S. J. Sherwin. Parametric uncertainty analysis of pulse wave propagation in a model of a human arterial network. *Journal of Computational Physics*, 226(2):1385–1407, 2007.

[2] K. H. Parker. A brief history of arterial wave mechanics. *Medical & Biological Engineering & Computing*, 47(2):111–118, 2009.

[3] T. J. Pedley. *The Fluid Mechanics of Large Blood Vessels*. Cambridge University Press, Cambridge, 1980.

[4] M. J. Lighthill and J. Lighthill. *Waves in Fluids*. Cambridge University Press, Cambridge, 2001.

[5] A. Lucca, S. Busto, L. O. Müller, E. F. Toro, and M. Dumbser. A semi-implicit finite volume scheme for blood flow in elastic and viscoelastic vessels. *Journal of Computational Physics*, 495:112530, 2023.

[6] H. G. Abdelwahed, M. A. Abdelrahman, A. F. Alsarhan, and K. Mohamed. Numerical simulating the blood flow model via nonhomogeneous riemann solver scheme. *Partial Differential Equations in Applied Mathematics*, 11:100845, 2024.

[7] S. Jana and S. Kuila. Riemann solutions of two-layered blood flow model in arteries. *International Journal of Non-Linear Mechanics*, 156:104485, 2023.

[8] Q. Zhang, W. Sheng, and T. Xiao. Riemann problem and godunov-type scheme for a two-layer blood flow model. *Applied Mathematics Letters*, 135:108437, 2023.

[9] R. Mondal, M. Minhajul, and T. Raja Sekhar. Interactions between elementary waves and weak discontinuity in two-layer blood flow through artery. *Physics of Fluids*, 36(3), 2024.

[10] S. Jana and S. Kuila. On the riemann problem and interaction of elementary waves for two-layered blood flow model through arteries. *Mathematical Methods in the Applied Sciences*, 47(1):27–46, 2024.

[11] B. Ghitti, C. Berthon, M. H. Le, and E. F. Toro. A fully well-balanced scheme for the 1d blood flow equations with friction source term. *Journal of Computational Physics*, 421:109750, 2020.

[12] G. I. Montecinos, A. Santacá, M. Celant, L. O. Müller, and E. F. Toro. Ader scheme with a simplified solver for the generalized riemann problem and an average eno reconstruction procedure. application to blood flow. *Computers & Fluids*, 248:105685, 2022.

[13] S. Shagolshem, B. Bira, and K. V. Nagaraja. Analysis of shock wave propagation in two-layered blood flow model via lie symmetry. *International Journal of Non-Linear Mechanics*, page 104761, 2024.

[14] W. Sheng and S. Xu. The riemann problem for the blood flow model with body force term. *Advances in Mathematical Physics*, 2024(1):2992241, 2024.

[15] J. Alastruey, K. H. Parker, J. Peiró, and S. J. Sherwin. Lumped parameter outflow models for 1-d blood flow simulations: Effect on pulse waves and parameter estimation. *Communications in Computational Physics*, 4(2):317–336, 2008.

[16] M. Willemet, V. Lacroix, and E. Marchandise. Inlet boundary conditions for blood flow simulations in truncated arterial networks. *Journal of Biomechanics*, 44(5):897–903, 2011.

[17] E. Marchandise, N. Chevaugeon, and J. F. Remacle. Spatial and spectral super convergence of discontinuous galerkin method for hyperbolic problems. *Journal of Computational and Applied Mathematics*, 215(2):484–494, 2008.

[18] M. A. Fernández, J. F. Gerbeau, and C. Grandmont. A projection semi-implicit scheme for the coupling of an elastic structure with an incompressible fluid. *Interna-*

tional Journal for Numerical Methods in Engineering, 69(4):794–821, 2007.

[19] F. N. Van de Vosse, J. De Hart, C. H. G. A. Van Oijen, D. Bessems, T. W. M. Gunther, A. Segal, and F. P. T. Baaijens. Finite-element-based computational methods for cardiovascular fluid-structure interaction. *Journal of Engineering Mathematics*, 47(3-4):335–368, 2003.

[20] Y. Watanabe, T. Asada, P. Y. Lagre, M. Saito, Y. Ikenaga, and M. Matsukawa. One-dimensional model for propagation of a pressure wave in a model of the human arterial network: Comparison of theoretical and experimental. *Journal of Biomechanical Engineering*, 2011.

[21] M. S. Olufsen, C. S. Peskin, W. Y. Kim, E. M. Pedersen, A. Nadim, and J. Larsen. Numerical simulation and experimental validation of blood flow in arteries with structured-tree outflow conditions. *Annals of Biomedical Engineering*, 28(11):1281–1299, 2000.

[22] J. M. Fullana and S. Zaleski. A branched one-dimensional model of vessel networks. *Journal of Fluid Mechanics*, 621:183–204, 2009.

[23] H. Tao, R. Husam, J. J. Dheyaa, K. S. Pradeep, F-H. A. Ali, H. A. H. Abbas, F. H. Dheyaa, M. Hiba, H. I. Ameer, and S. S. S. Narinderjit. Computational analysis of pulsatile blood flow and heat transport dynamics in middle cerebral artery aneurysms in different body physiologies. *International Journal of Modern Physics C*, 36(6):2450236, 2025.

[24] B. St Venant. Theory of the non-permanent movement of the waters with application to the floods of the rivers and to the introduction of the marees in their bed. *Comptes Rendus de l'Académie des Sciences*, 73:148–154, 1871.

[25] J. Burguete, P. García-Navarro, and J. Murillo. Friction term discretization and limitation to preserve stability and conservation in the 1d shallow water model: Application to unsteady irrigation and river flow. *International Journal for Numerical Methods in Fluids*, 58(4):403–425, 2008.

[26] A. Valiani, V. Caleffi, and A. Zanni. Finite volume scheme for 2d shallow-water equations. application to the malpasset dam-break. In *The 4th CADAM Workshop, Zaragoza*, pages 63–94, November 1999.

[27] A. Valiani, V. Caleffi, and A. Zanni. Case study: Malpasset dam-break simulation using a two-dimensional finite volume method. *Journal of Hydraulic Engineering*, 128(5):460–472, 2002.

[28] S. Popinet. Quadtree-adaptive tsunami modelling. *Ocean Dynamics*, 61(9):1261–1285, 2011.

[29] A. Bermudez and M. E. Vázquez. Upwind methods for hyperbolic conservation laws with source terms. *Computers & Fluids*, 23(8):1049–1071, 1994.

[30] A. Bermúdez, A. Dervieux, J. A. Desideri, and M. E. Vázquez. Upwind schemes for the two-dimensional shallow water equations with variable depth using unstructured meshes. *Computer Methods in Applied Mechanics and Engineering*, 155(1-2):49–72, 1998.

[31] R. J. LeVeque. *Finite Volume Methods for Hyperbolic Problems*, volume 31. Cambridge University Press, Cambridge, 2002.

[32] S. Jin. A steady-state capturing method for hyperbolic systems with geometrical source terms. *ESAIM: Mathematical Modelling and Numerical Analysis*, 35(4):631–645, 2001.

[33] L. Gosse. A well-balanced flux-vector splitting scheme designed for hyperbolic systems of conservation laws with source terms. *Computers & Mathematics with Applications*, 39(9-10):135–159, 2000.

[34] T. Gallout, J. M. Hérard, and N. Seguin. Some approximate godunov schemes to compute shallow-water equations with topography. *Computers & Fluids*, 32(4):479–513, 2003.

[35] O. Delestre, A. Ghigo, J. M. Fullana, and P. Y. Lagrée. A shallow water with variable pressure model for blood flow simulation. arXiv preprint arXiv:1509.01917, 2015.

[36] O. Delestre and P. Y. Lagrée. A well-balanced finite volume scheme for blood flow simulation. *International Journal for Numerical Methods in Fluids*, 72(2):177–205, 2013.

[37] G. Li, O. Delestre, and L. Yuan. Well-balanced discontinuous galerkin method and finite volume weno scheme based on hydrostatic reconstruction for blood flow model in arteries. *International Journal for Numerical Methods in Fluids*, 86(7):491–508, 2018.

[38] S. C. Chang. The method of space-time conservation element and solution element: A new approach for solving the navier–stokes and euler equations. *Journal of Computational Physics*, 119(2):295–324, 1995.

[39] S. C. Chang, X. Y. Wang, and C. Y. Chow. New developments in the method of space-time conservation element and solution element: Applications to two-dimensional time-marching problems, 1994.

[40] S. C. Chang, X. Y. Wang, and C. Y. Chow. The space-time conservation element and solution element method: A new high-resolution and genuinely multidimensional paradigm for solving conservation laws. *Journal of Computational Physics*, 156(1):89–136, 1999.

[41] S. C. Chang, X. Y. Wang, and W. M. To. Application of the space-time conservation element and solution element method to one-dimensional convection diffusion problems. *Journal of Computational Physics*, 165(1):189–215, 2000.

[42] M. Liu, J. B. Wang, and K. Q. Wu. The direct aero-acoustics simulation of flow around a square cylinder using the ce/se scheme. *Journal of Algorithms & Computational Technology*, 1(4):525–538, 2007.

[43] C. Y. Loh and K. B. M. Q. Zaman. Numerical investigation of transonic resonance with a convergent-divergent nozzle. *AIAA Journal*, 40(12):2393–2401, 2002.

[44] C. Y. Loh, L. S. Hultgren, and S. C. Chang. Wave computation in compressible flow using space-time conservation element and solution element method. *AIAA Journal*, 39(5):794–801, 2001.

[45] C. Loh, S. C. Chang, P. Jorgenson, and L. Hultgren. Noise computation of a shock-containing supersonic axisymmetric jet by the ce/se method. In *38th Aerospace Sciences Meeting and Exhibit*, page 475, December 1999.

[46] S. Qamar and S. Mudasser. On the application of a variant ce/se method for solving

two-dimensional ideal mhd equations. *Applied Numerical Mathematics*, 60(6):587–606, 2010.

[47] X. Y. Wang, C. L. Chen, and Y. Liu. The space-time ce/se method for solving maxwell's equations in time-domain. In *IEEE Antennas and Propagation Society International Symposium*, volume 1, pages 164–167. IEEE, June 2002.

[48] H. Nessyahu and E. Tadmor. Non-oscillatory central differencing for hyperbolic conservation laws. *Journal of Computational Physics*, 87(2):408–463, 1990.

[49] L. Formaggia, A. Quarteroni, and A. Veneziani. Cardiovascular mathematics: Modeling and simulation of the circulatory system. 2009.

[50] M. S. Olufsen. A one-dimensional fluid dynamic model of the systemic arteries. *American Journal of Physiology-Heart and Circulatory Physiology*, 276(1):H257–H268, 2000.

[51] N. Wei, C. Xu, Y. Meng, G. Li, M. Xiao, and A. Liu. Numerical simulation of gas-liquid two-phase flow in wellbore based on drift flux model. *Applied Mathematics and Computation*, 338:175–191, 2018.

[52] O. Delestre, C. Lucas, P. A. Ksinant, F. Darboux, C. Laguerre, T. N. T. Vo, and S. Cordier. Swashes: A compilation of shallow water analytic solutions for hydraulic and environmental studies. *International Journal for Numerical Methods in Fluids*, 72(3):269–300, 2013.

[53] J. R. Womersley. XXIV. oscillatory motion of a viscous liquid in a thin-walled elastic tube: The linear approximation for long waves. *The London, Edinburgh, and Dublin Philosophical Magazine and Journal of Science*, 46(373):199–221, 1955.